Journal of Solid State Chemistry **158,** 299–306 (2001)
doi:10.1006/jssc.2001.9110, available online at http://www.idealibrary.com on IDEAL®

Syntheses, Structures, and Physical Properties of the New Quaternary Rare-Earth Chalcogenides $RbNd_2CuS_4$, $RbSm_2CuS_4$, $CsLa_2CuSe_4$, $CsSm_2CuSe_4$, $RbEr_2Cu_3S_5$, $CsGd_2Ag_3Se_5$, $CsTb_2Ag_3Se_5$, and $Rb_2Gd_4Cu_4S_9$

Fu Qiang Huang and James A. Ibers

Department of Chemistry, Northwestern University, 2145 Sheridan Road, Evanston, Illinois 60208-3113

Received October 24, 2000; in revised form January 10, 2001; accepted January 19, 2001

Eight quaternary rare-earth chalcogenides, $RbNd_2CuS_4$, $RbSm_2CuS_4$, $CsLa_2CuSe_4$, $CsSm_2CuSe_4$, $RbEr_2Cu_3S_5$, $CsGd_2Ag_3Se_5$, $CsTb_2Ag_3Se_5$, and $Rb_2Gd_4Cu_4S_9$, have been synthesized at 973 K with the use of a reactive flux of A_2Q_3 (A = Rb, Cs; Q = S, Se). All structural data were obtained at 153 K. The isostructural compounds ALn_2CuQ_4 (Ln = rare earth) crystallize with four formula units in the KGd_2CuS_4 structure type in space group *Cmcm* of the orthorhombic system; the isostructural compounds $ALn_2M_3Q_5$ (M = Cu, Ag) crystallize with four formula units in the $RbSm_2Ag_3Se_5$ structure type in space group *Cmcm* of the orthorhombic system; and $Rb_2Gd_4Cu_4S_9$ crystallizes with two formula units in space group $C2/m$ of the monoclinic system. The cell dimensions of ALn_2CuQ_4 (a, b, c (Å)) are as follows: $RbNd_2CuS_4$, 4.0762(3), 13.954(1), 13.964(1); $RbSm_2CuS_4$, 4.0391(3), 13.815(1), 13.860(1); $CsLa_2CuSe_4$, 4.3129(6), 14.959(2), 14.798(2); $CsSm_2CuSe_4$, 4.2066(3), 14.6101(9), 14.5164(9). The corresponding R_1 indices for the refined structures are 0.0264, 0.0196, 0.0258, and 0.0224. The cell dimensions of $ALn_2M_3Q_5$ are as follows: $RbEr_2Cu_3S_5$, 3.9283(3), 13.897(1), 16.348(1); $CsGd_2Ag_3Se_5$, 4.2943(4), 15.424(1), 17.501(2); $CsTb_2Ag_3Se_5$, 4.2779(4), 15.429(2), 17.426(2). The R_1 indices are 0.0257, 0.0255, and 0.0241. The cell dimensions of $Rb_2Gd_4Cu_4S_9$ (a, b, c (Å), β (°)) is 13.897(1), 3.9883(3), 16.054(1), 109.273(1), and the R_1 index is 0.0199. All eight compounds have closely related three-dimensional tunnel structures. All alkali metal atoms in the tunnels are coordinated to eight Q atoms. Their anionic frameworks are built from LnQ_6 octahedra and MQ_4 tetrahedra. ALn_2CuQ_4 contains $^1_\infty[CuQ_3]$ chains of vertex-sharing tetrahedra; $Rb_2Gd_4Cu_4S_9$ contains $^1_\infty[Cu_4S_8]$ chains of tetrahedra; and $ALn_2M_3Q_5$ contains $^2_\infty[M_3Q_5]$ layers of tetrahedra. $Rb_2Gd_4Cu_4S_9$ and $RbEr_2Cu_3S_5$, which are paramagnetic, obey the Curie–Weiss law, and have effective magnetic moments of 7.9(2) μ_B for Gd^{3+} and 9.43(5) μ_B for Er^{3+}. A band gap of 1.94 eV for $Rb_2Gd_4Cu_4S_9$ was deduced from its diffuse reflectance spectrum, and the typical $4f$–$4f$ optical transitions for Er^{3+} were found in $RbEr_2Cu_3S_5$ at about 1.6, 1.9, and 2.5 eV.

INTRODUCTION

A number of $A/Ln/M/Q$ (A = s-block metal; Ln = f-block element, usually a rare earth; M = d-block element; Q = chalcogen = S, Se, Te) systems have been synthesized, since the development of the reactive flux method (1, 2). These include $RbLn_2CuSe_4$ (Ln = Sm, Gd, Dy) (3), $Rb_{1.5}Ln_2Cu_{2.5}Se_5$ (Ln = Gd, Dy) (3), $RbSm_2Ag_3Se_5$ (3), $CsUTiTe_5$ (4), $BaLnMQ_3$ (Ln = rare-earth; M = Cu, Ag, Au; Q = S, Se, Te) (5–8), $Ba_2LnAg_5S_6$ (Ln = La, Y) (9), $K_{1.5}Dy_2Cu_{2.5}Te_5$ (8), $K_{0.5}Ba_{0.5}DyCu_{1.5}Te_3$ (8), KGd_2CuS_4 (10), $K_2CeCu_2S_4$ (11), $ALnCu_2S_6$ (A = K, Cs; Ln = La, Ce, Eu) (11–13), $ALnCuQ_3$ (A = K, Cs; Ln = Ce, U; Q = S, Se, Te) (4, 13), $K_2CeAg_3Te_4$ (14), $KCeCuTe_4$ (15), and $Rb_2CeCu_3Te_5$ (16). These compounds crystallize in a variety of structure types that include two-dimensional layered structures and three-dimensional tunnel structures. The M atoms (except Ti) are tetrahedrally coordinated by chalcogen atoms. These tetrahedra enter into chains, layers, and other frameworks. The compounds $ALnCu_2S_6$, $KCeCuTe_4$, and $Rb_2CeCu_3Te_5$ all contain Q–Q bonds and have layered structures. The coordination environment of these Ln atoms are bicapped or tricapped trigonal prisms. In the compounds without Q–Q bonding interactions, each Ln atom is coordinated to an octahedron of six Q atoms. These compounds provide considerable information about how diverse chalcogenide structures are constructed from octahedra and tetrahedra.

Here we report the syntheses and structural characterization of eight new compounds containing f- and d-block metals, namely $RbNd_2CuS_4$, $RbSm_2CuS_4$, $CsLa_2CuSe_4$, $CsSm_2CuSe_4$, $RbEr_2Cu_3S_5$, $CsGd_2Ag_3Se_5$, $CsTb_2Ag_3Se_5$, and $Rb_2Gd_4Cu_4S_9$. They all possess three-dimensional structures containing similar tunnels. In addition, we report the magnetic and optical properties of $Rb_2Gd_4Cu_4S_9$ and $RbEr_2Cu_3S_5$.

0022-4596/01 $35.00

TABLE 1
Crystal Data and Structure Refinement for $RbNd_2CuS_4$, $RbSm_2CuS_4$, $CsLa_2CuSe_4$, $CsSm_2CuSe_4$, $RbEr_2Cu_3S_5$, $CsGd_2Ag_3Se_5$, $CsTb_2Ag_3Se_5$, and $Rb_2Gd_4Cu_4S_9$[a]

Compound	$RbNd_2CuS_4$	$RbSm_2CuS_4$	$CsLa_2CuSe_4$	$CsSm_2CuSe_4$	$RbEr_2Cu_3S_5$	$CsGd_2Ag_3Se_5$	$CsTb_2Ag_3Se_5$	$Rb_2Gd_4Cu_4S_9$
Formula weight	565.73	577.95	790.11	812.99	770.91	1165.82	1169.16	1342.64
a (Å)	4.0762(3)	4.0391(3)	4.3129(6)	4.2066(3)	3.9283(3)	4.2943(4)	4.2779(4)	13.897(1)
b (Å)	13.954(1)	13.815(1)	14.959(2)	14.6101(9)	13.897(1)	15.424(1)	15.429(2)	3.9883(3)
c (Å)	13.964(1)	13.860(1)	14.798(2)	14.5164(9)	16.348(1)	17.501(2)	17.426(2)	16.054(1)
β (°)	90	90	90	90	90	90	90	109.273(1)
Space group	*Cmcm*	*Cmcm*	*Cmcm*	*Cmcm*	*Cmcm*	*Cmcm*	*Cmcm*	*C2/m*
Z	4	4	4	4	4	4	4	2
V	794.3(1)	773.4(1)	954.7(2)	892.2(1)	892.5(1)	1159.2(2)	1150.2(2)	839.9(1)
ρ_c (g/cm^3)	4.731	4.964	5.497	6.053	5.738	6.680	6.752	5.309
μ (cm^{-1})	225.66	249.33	299.14	355.99	321.36	349.93	360.33	273.61
Transm factors	0.364–0.555	0.152–0.399	0.233–0.325	0.082–0.191	0.208–0.397	0.328–0.509	0.390–0.514	0.220–0.451
R_1[b]	0.0264	0.0196	0.0258	0.0224	0.0257	0.0255	0.0241	0.0199
wR_2[c]	0.0668	0.0517	0.0701	0.0617	0.0626	0.0566	0.0591	0.0534

[a] For all structures $T = 153$ K and $\lambda = 0.71073$ Å.
[b] $R_1 = \sum||F_o| - |F_c||/|F_o|$; $F_o^2 > 2\sigma(F_o^2)$.
[c] $wR_2 = \{\sum[w(F_o^2 - F_c^2)^2]/\sum wF_o^4\}^{1/2}$; $w^{-1} = \sigma^2(F_o^2) + (0.04 \times F_o^2)^2$ for $F_o^2 \geq 0$ and $w^{-1} = \sigma^2(F_o^2)$ for $F_o^2 < 0$.

TABLE 2
Atomic Coordinates[a] and Equivalent Isotropic Displacement Parameters (Å^2) for $RbNd_2CuS_4$, $RbSm_2CuS_4$, $CsLa_2CuSe_4$, and $CsSm_2CuSe_4$

Atom	y	z	U_{eq}[b]
$RbNd_2CuS_4$			
Rb	0.10667(5)	$\frac{1}{4}$	0.0101(2)
Nd	0.36580(2)	0.06141(2)	0.0064(2)
Cu	0.83517(7)	$\frac{1}{4}$	0.0092(2)
S1	0.26115(9)	0.61141(9)	0.0070(3)
S2	0.4255(1)	$\frac{1}{4}$	0.0070(4)
S3	0	0	0.0094(4)
$RbSm_2CuS_4$			
Rb	0.10719(4)	$\frac{1}{4}$	0.0092(2)
Sm	0.36588(1)	0.06153(2)	0.0058(1)
Cu	0.83516(6)	$\frac{1}{4}$	0.0084(2)
S1	0.26108(8)	0.61026(7)	0.0067(2)
S2	0.4256(1)	$\frac{1}{4}$	0.0067(3)
S3	0	0	0.0084(3)
$CsLa_2CuSe_4$			
Cs	0.10560(4)	$\frac{1}{4}$	0.0100(2)
La	0.36548(3)	0.06068(2)	0.0065(2)
Cu	0.83478(8)	$\frac{1}{4}$	0.0110(3)
Se1	0.26027(4)	0.61220(5)	0.0069(2)
Se2	0.42193(6)	$\frac{1}{4}$	0.0072(2)
Se3	0	0	0.0092(2)
$CsSm_2CuSe_4$			
Cs	0.10720(4)	$\frac{1}{4}$	0.0114(2)
Sm	0.36592(2)	0.06125(2)	0.0090(2)
Cu	0.83369(8)	$\frac{1}{4}$	0.0123(3)
Se1	0.25978(4)	0.60841(4)	0.0093(2)
Se2	0.42192(6)	$\frac{1}{4}$	0.0095(2)
Se3	0	0	0.0107(2)

[a] The x coordinate of all atoms is 0.
[b] U_{eq} is defined as one third of the trace of the orthogonalized U_{ij} tensor.

EXPERIMENTAL

Syntheses

The following reagents were used as obtained: Rb (Aldrich, 98 + %), Cs (Aldrich, 99.5%), La (Alfa, 99.9%), Nd (Alfa, 99.9%), Sm (Alfa, 99.9%), Gd (Alfa, 99.9%), Tb (Aldrich, 99.9%), Er (Alfa, 99.9%), Cu (Aldrich, 99.999%), Ag (Alfa, 99.99%), S (Alfa, 99.5%), and Se (Aldrich, 99.5%). A_2Q_3 (A = Rb, Cs; Q = S, Se), the reactive fluxes (1) employed in the syntheses, were prepared by

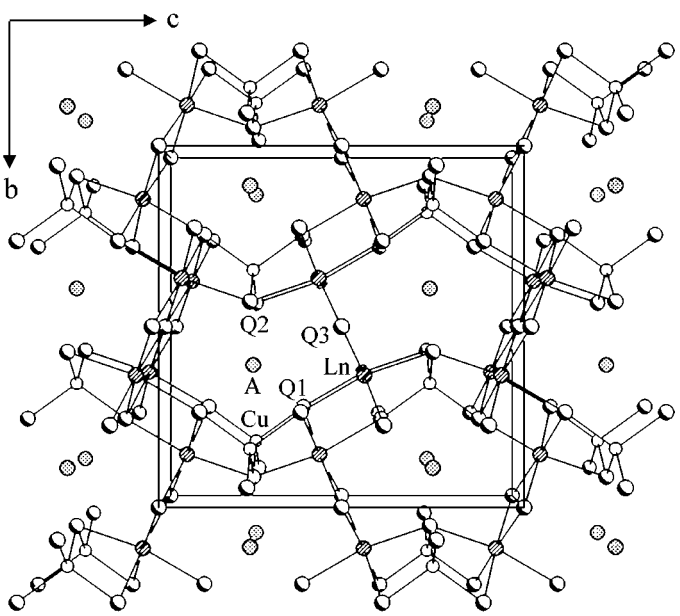

FIG. 1. Unit cell of ALn_2CuQ_4 viewed down in [100].

TABLE 3
Atomic Coordinates[a] and Equivalent Isotropic Displacement Parameters (Å^2) for $RbEr_2Cu_3S_5$, $CsGd_2Ag_3Se_5$, and $CsTb_2Ag_3Se_5$

Atom	y	z	U_{eq}
$RbEr_2Cu_3S_5$			
Rb	0.43407(6)	$\frac{1}{4}$	0.0096(2)
Er	0.30771(2)	0.59379(2)	0.0061(2)
Cu1	0.15201(8)	$\frac{1}{4}$	0.0108(3)
Cu2	0.08220(5)	0.53943(5)	0.0112(2)
S1	0.0628(1)	0.1151(1)	0.0069(3)
S2	0.7407(1)	$\frac{1}{4}$	0.0070(4)
S3	0.3299(1)	0.0694(1)	0.0068(3)
$CsGd_2Ag_3Se_5$			
Cs	0.43810(5)	$\frac{1}{4}$	0.0129(2)
Gd	0.30746(3)	0.59525(2)	0.0088(1)
Ag1	0.15584(7)	$\frac{1}{4}$	0.0126(2)
Ag2	0.08265(5)	0.54101(4)	0.0140(2)
Se1	0.06742(5)	0.11654(5)	0.0092(2)
Se2	0.75264(8)	$\frac{1}{4}$	0.0095(3)
Se3	0.31952(6)	0.07026(5)	0.0089(2)
$CsTb_2Ag_3Se_5$			
Cs	0.43850(5)	$\frac{1}{4}$	0.0121(2)
Tb	0.30705(2)	0.59531(2)	0.0082(1)
Ag1	0.15577(6)	$\frac{1}{4}$	0.0122(2)
Ag2	0.08222(4)	0.54205(4)	0.0129(2)
Se1	0.06855(5)	0.11624(4)	0.0086(2)
Se2	0.75310(7)	$\frac{1}{4}$	0.0091(2)
Se3	0.31894(5)	0.06989(4)	0.0083(2)

[a]The x coordinate of all atoms is 0.

stoichiometric reactions of the elements in liquid NH_3. The reaction mixtures were (A_2Q_3, Ln, M, Q in mmol): ALn_2CuQ_4 (1.2, 1.0, 0.5, 2.0), $ALn_2M_3Q_5$ (1.2, 1.0, 1.0, 3.0), and $Rb_2Gd_4Cu_4S_9$ (1.5, 2.0, 2.0, 5.0). These mixtures were loaded into fused-silica tubes under an Ar atmosphere in a glove box. These tubes were sealed under a 10^{-4} Torr atmosphere and then placed in a computer-controlled furnace. The samples were heated to 973 K in 15 h, kept at 973 K for 3 days, slowly cooled at 10 K/h to 473 K, and then cooled to room temperature. Major products in all instances were red (ALn_2CuQ_4 and $Rb_2Gd_4Cu_4S_9$) or brown ($ALn_2M_3Q_5$) needles of the desired materials. Yields varied from 70 to 90%. Selected single crystals were examined with an EDX-equipped Hitachi S-4500 SEM and found to have the stated compositions within the accuracy of the method ($\pm$ 5%). All these compounds are modestly stable in air.

TABLE 4
Atomic Coordinates[a] and Equivalent Isotropic Displacement Parameters (Å^2) for $Rb_2Gd_4Cu_4S_9$

Atom	x	z	U_{eq}
Rb	0.02799(4)	0.76965(3)	0.0107(1)
Gd1	0.23221(2)	0.60443(2)	0.0066(1)
Gd2	0.65408(2)	0.05370(2)	0.0069(1)
Cu1	0.24845(6)	0.22924(5)	0.0109(2)
Cu2	0.43260(6)	0.54142(5)	0.0121(2)
S1	0.1394(1)	0.42523(9)	0.0071(3)
S2	0.2978(1)	0.10142(9)	0.0075(3)
S3	0.3916(1)	0.37451(9)	0.0078(3)
S4	0.6558(1)	0.22218(9)	0.0079(3)
S5	0	0	0.0093(4)

[a]The y coordinate of all atoms is 0.

TABLE 5
Selected Bond Distances (Å) for $RbNd_2CuS_4$, $RbSm_2CuS_4$, $CsLa_2CuSe_4$, and $CsSm_2CuSe_4$

	$RbNd_2CuS_4$	$RbSm_2CuS_4$	$CsLa_2CuSe_4$	$CsSm_2CuSe_4$
A–$Q1 \times 4$	3.362(1)	3.3379(9)	3.5825(7)	3.5250(6)
A–$Q2 \times 2$	3.247(2)	3.221(1)	3.4928(9)	3.4281(8)
A–$Q3 \times 2$	3.7951(4)	3.7682(3)	4.0227(5)	3.9527(3)
Ln–$Q1 \times 2$	2.7892(9)	2.7589(7)	2.9614(6)	2.8749(4)
Ln–$Q1$	2.821(1)	2.787(1)	3.0036(8)	2.9105(7)
Ln–$Q2$	2.7622(7)	2.7394(6)	2.9261(6)	2.8595(4)
Ln–$Q3 \times 2$	2.8976(2)	2.8704(2)	3.0832(4)	3.0086(3)
Cu–$Q1 \times 2$	2.356(1)	2.349(1)	2.486(1)	2.4676(9)
Cu–$Q2 \times 2$	2.397(1)	2.375(1)	2.5199(8)	2.4669(8)

Crystallography

Single-crystal X-ray diffraction data were obtained with the use of graphite-monochromatized Mo$K\alpha$ radiation ($\lambda = 0.71073$ Å) at 153 K on a Bruker Smart-1000 CCD diffractometer (17). The crystal-to-detector distance was 5.023 cm. Crystal decay was monitored by recollecting 50 initial frames at the end of data collection. Data were collected by a scan of 0.3° in ω in groups of 606, 606, and 606 frames at φ settings of 0°, 120°, and 240° for all the compounds except $CsSm_2CuSe_4$ for which 606, 606, 606, and

TABLE 6
Selected Bond Distances (Å) for $RbEr_2Cu_3S_5$, $CsGd_2Ag_3Se_5$, and $CsTb_2Ag_3Se_5$

	$RbEr_2Cu_3S_5$	$CsGd_2Ag_3Se_5$	$CsTb_2Ag_3Se_5$
A–$Q1 \times 4$	3.453(1)	3.7475(8)	3.7463(8)
A–$Q2 \times 2$	3.228(2)	3.577(1)	3.572(1)
A–$Q3 \times 2$	3.388(2)	3.639(1)	3.6406(9)
Ln–$Q1 \times 2$	2.686(1)	2.9109(7)	2.8970(6)
Ln–$Q2$	2.6409(6)	2.8626(6)	2.8509(6)
Ln–$Q3$	2.6858(2)	2.902(1)	2.8846(9)
Ln–$Q3 \times 2$	2.770(1)	2.9390(7)	2.9240(6)
$M1$–$Q1 \times 2$	2.530(2)	2.705(1)	2.6915(9)
$M1$–$Q2 \times 2$	2.319(1)	2.6152(9)	2.6135(8)
$M2$–$Q1$	2.364(2)	2.665(1)	2.661(1)
$M2$–$Q1$	2.540(2)	2.767(1)	2.766(1)
$M2$–$Q3 \times 2$	2.364(1)	2.6738(7)	2.6713(6)

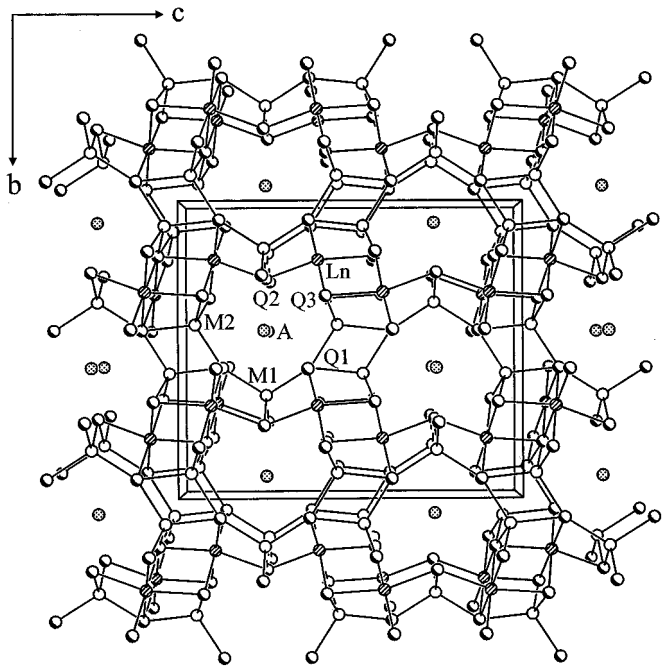

FIG. 2. Unit cell of $ALn_2M_3Q_5$ viewed down [100].

606 frames at φ settings of 0°, 90°, 180°, and 270° were collected. The exposure times were 15 s/frame for all the compounds. The collection of intensity data on the Bruker diffractometer was carried out with the program SMART (17). Cell refinement and data reduction were carried out with the use of the program SAINT (17) and face-indexed absorption corrections were carried out numerically with the program XPREP (18). Then the program SADABS (17) was employed to make incident beam and decay corrections.

TABLE 7
Selected Bond Distances (Å) for $Rb_2Gd_4Cu_4S_9$

Rb–S1	3.224(1)	Gd2–S2	2.783(1)
Rb–S2 × 2	3.289(1)	Gd2–S4	2.697(1)
Rb–S3 × 2	3.506(1)	Gd2–S5 × 2	2.8437(2)
Rb–S4 × 2	3.277(1)	Cu1–S2	2.369(2)
Rb–S5	3.8439(6)	Cu1–S3	2.516(1)
Gd1–S1	2.737(1)	Cu1–S4 × 2	2.3562(9)
Gd1–S1 × 2	2.819(1)	Cu2–S1 × 2	2.3706(8)
Gd1–S3 × 2	2.726(1)	Cu2–S3	2.370(2)
Gd1–S4	2.704(1)	Cu2–S3	2.549(1)
Gd2–S2 × 2	2.746(1)		

The structures were solved with the direct methods program SHELXS and refined with the full-matrix least-squares program SHELXL of the SHELXTL-PC suite of programs (18). Each final refinement included anisotropic displacement parameters and a secondary extinction correction. Additional crystallographic details are given in Table 1. Tables 2, 3, and 4 give positional parameters and equivalent isotropic displacement parameters, and Tables 5, 6, and 7 present selected bond distances for $RbNd_2CuS_4$, $RbSm_2CuS_4$, $CsLa_2CuSe_4$, $CsSm_2CuSe_4$, $RbEr_2Cu_3S_5$, $CsGd_2Ag_3Se_5$, $CsTb_2Ag_3Se_5$, and $Rb_2Gd_4Cu_4S_9$.

Magnetic Susceptibility

A 20-mg sample of $Rb_2Gd_4Cu_4S_9$ and a 15-mg sample of $RbEr_2Cu_3S_5$ containing single crystals were used for mag-

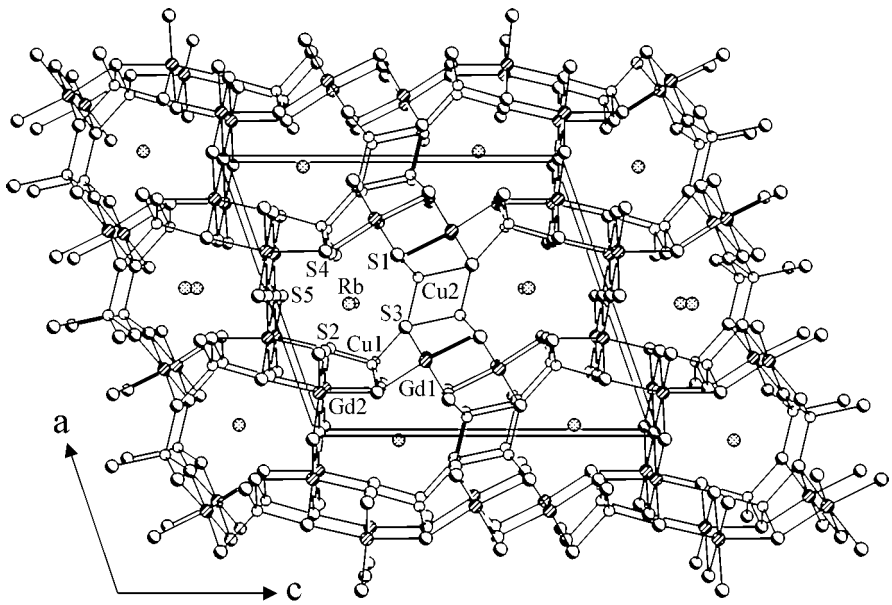

FIG. 3. Unit cell of $Rb_2Gd_4Cu_4S_9$ viewed down [010].

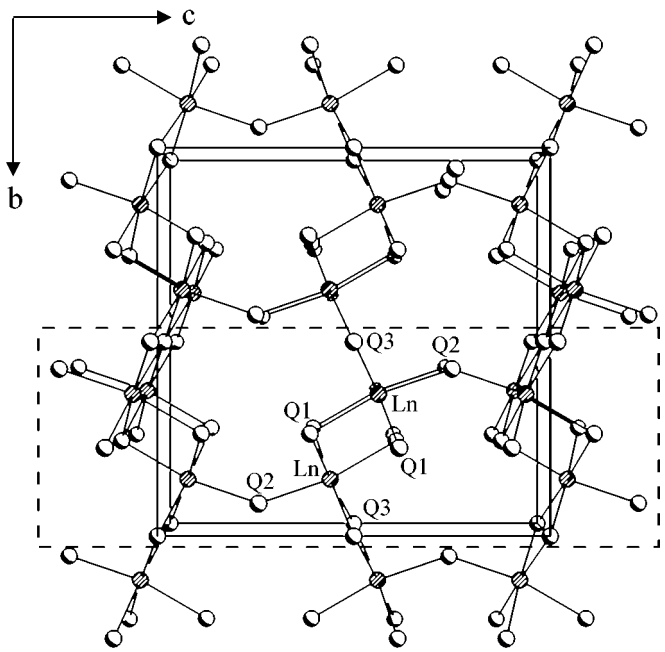

FIG. 4. The Ln/Q fragment of ALn_2CuQ_4 viewed down [100]. The $^2_\infty[Ln_2Q_5]$ layer is in the dashed box.

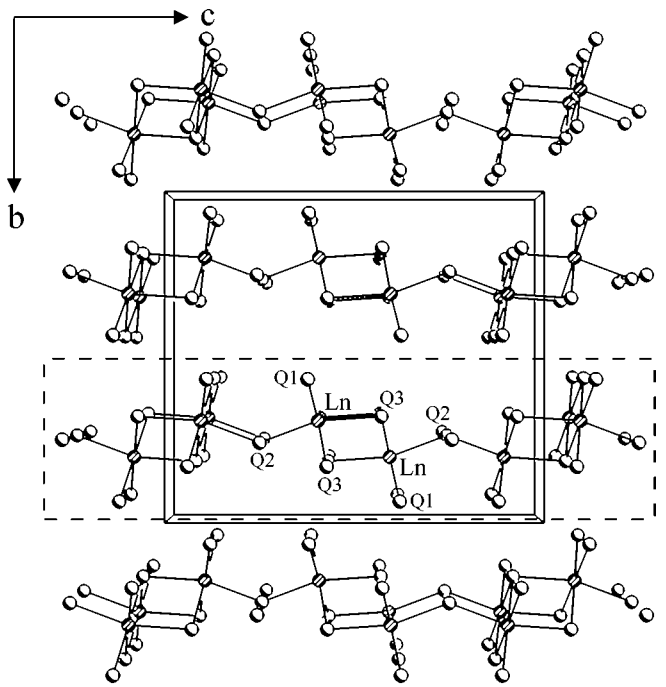

FIG. 6. The Ln/Q fragment of $ALn_2M_3Q_5$ viewed down [100]. The $^2_\infty[Ln_2Q_5]$ layer is in the dashed box.

netic susceptibility measurements. The composition of each sample was verified by EDX measurements. The magnetization was measured at 200 G between 5 and 300 K with the use of a Quantum Design SQUID magnetometer. All measurements were corrected for core diamagnetism (19).

UV–Vis Diffuse Reflectance Spectroscopy

A Cary 1E UV–visible spectrophotometer with a diffuse reflectance accessory was used to measure the diffuse reflectance spectra of the compounds $Rb_2Gd_4Cu_4S_9$ and $RbEr_2Cu_3S_5$ over the range 350 nm (3.54 eV) to 900 nm (1.38 eV) at 293 K.

RESULTS AND DISCUSSION

The structure of the isostructural compounds $RbNd_2CuS_4$, $RbSm_2CuS_4$, $CsLa_2CuSe_4$, and $CsSm_2CuSe_4$ is illustrated in Fig. 1. This is the KGd_2CuS_4 structure type

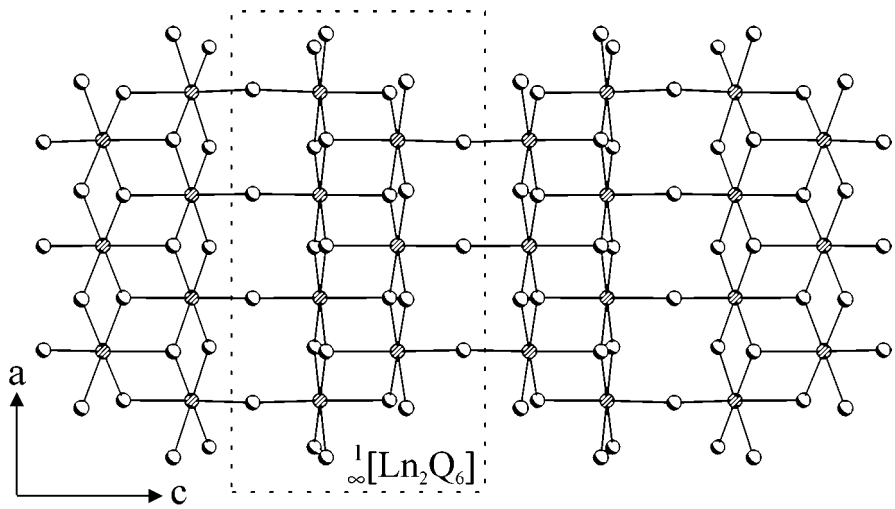

FIG. 5. The $^2_\infty[Ln_2Q_5]$ layer of $ALn_2M_3Q_5$ viewed down [010]. The $^1_\infty[Ln_2Q_6]$ chain is in the dashed box.

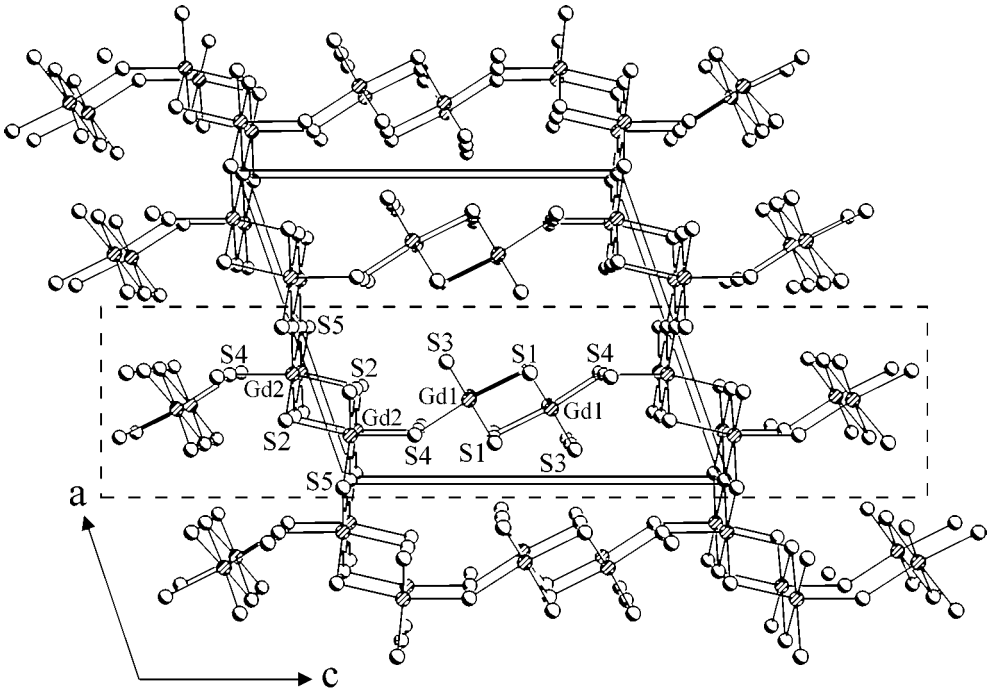

FIG. 7. The *Ln*/*Q* fragment of $Rb_2Gd_4Cu_4S_9$ viewed down [010]. The $^2_\infty[Ln_2Q_5]$ layer is in the dashed box.

(10). The structure of the isostructural compounds $RbEr_2Cu_3S_5$, $CsGd_2Ag_3Se_5$, and $CsTb_2Ag_3Se_5$ is illustrated in Fig. 2. This is the $RbSm_2Ag_3Se_5$ structure type (3). The structure of $Rb_2Gd_4Cu_4S_9$, a new structure type, is illustrated in Fig. 3. These three structures all have three-dimensional tunnel frameworks with similarly shaped tunnels. Each tunnel is only large enough in cross section to accommodate one *A* atom. The tunnel in ALn_2CuQ_4 comprises a 10-membered ring of two Cu–*Q* bonds and eight *Ln*–*Q* bonds, that in $ALn_2M_3Q_5$ consists of a 10-membered ring of six *M*–*Q* bonds and four *Ln*–*Q* bonds, and that in $Rb_2Gd_4Cu_4S_9$ consists of a 10-membered ring of four Cu–S bonds and six Gd–S bonds.

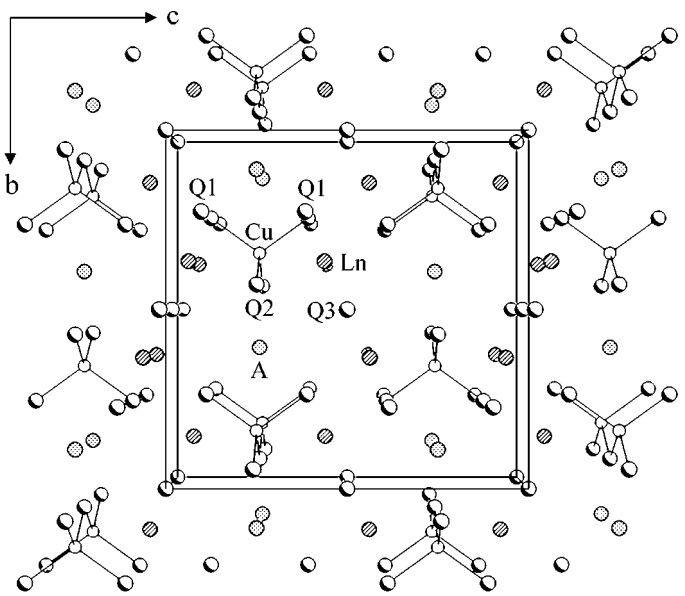

FIG. 8. Unit cell of ALn_2CuQ_4 viewed down [100] with only Cu–*Q* bonds shown.

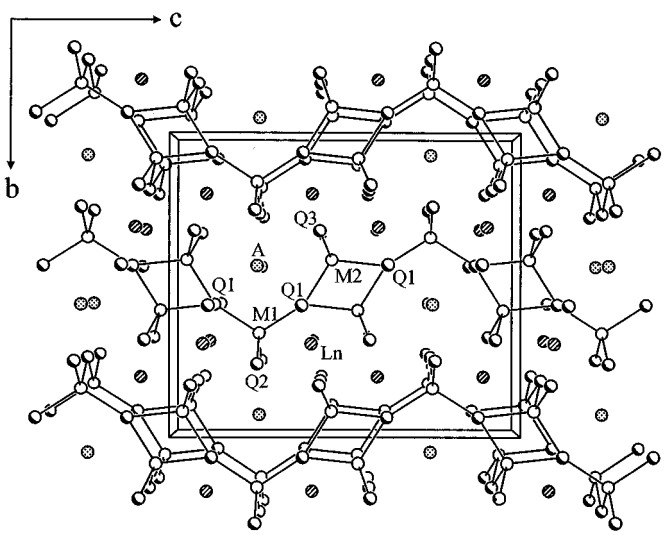

FIG. 9. Unit cell of $ALn_2M_3Q_5$ viewed down [100] with only *M*–*Q* bonds shown.

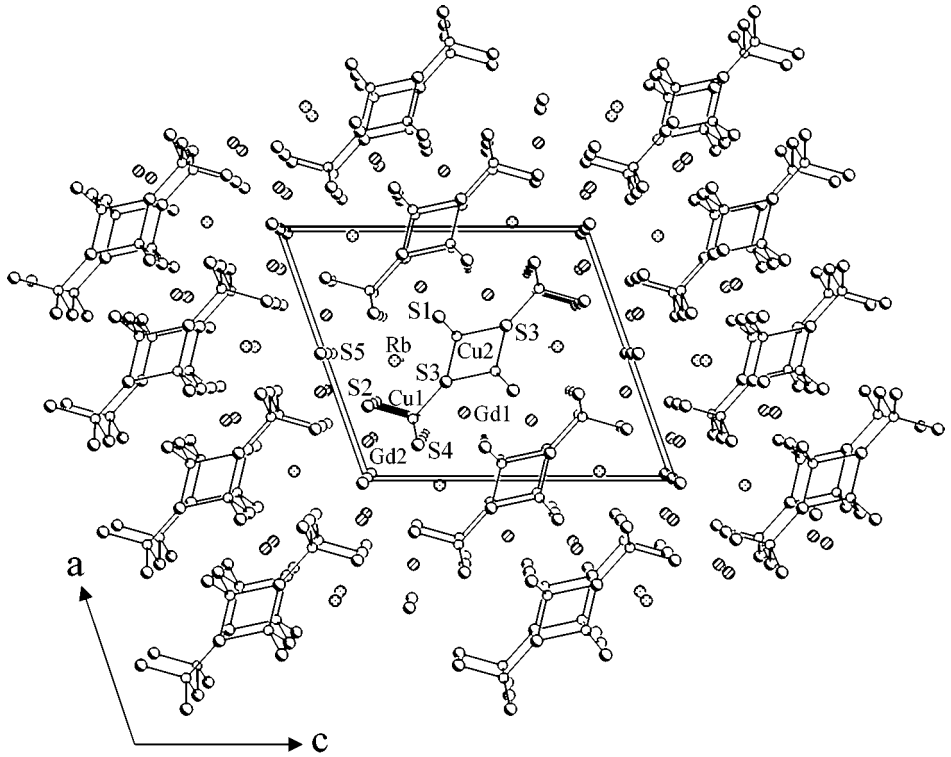

FIG. 10. Unit cell of $Rb_2Gd_4Cu_4S_9$ viewed down [010] with only Cu–S bonds shown.

The entire framework in each of the three structure can be derived topologically from the NaCl structure. When larger eight-coordinated *A* atoms and smaller four-coordinated *M* atoms replace some of the six-coordinated *Ln* atoms, the NaCl-like *Ln*/*Q* framework distorts. Some alkali-metal/rare-earth/chalcogenides, such as $ALnQ_2$ (20, 21), $CsEr_3Se_5$ (22), and $A_3Ln_7Se_{12}$ (22, 23), are three-dimensional NaCl-like tunnel structures built from LnQ_6.

The three-dimensional anionic frameworks in the three structures are built from LnQ_6 octahedra and MQ_4 tetrahedra, as shown in Figs. 1, 2, and 3. The *Ln*/*Q* fragments in these structures consist of similar $^2_\infty[Ln_2Q_5]$ layers, as shown in Figs. 4, 5, 6, and 7. As an example, the $^2_\infty[Ln_2Q_5]$ layer in $ALn_2M_3Q_5$ is displayed in Fig. 5. This layer is composed of $^1_\infty[Ln_2Q_6]$ chains along [100], which are built from the edge-sharing of LnQ_6 octahedra. These chains are connected to each other by the vertex-sharing of *Q* atoms to form the two-dimensional $^2_\infty[Ln_2Q_5]$ layer (Fig. 5). The

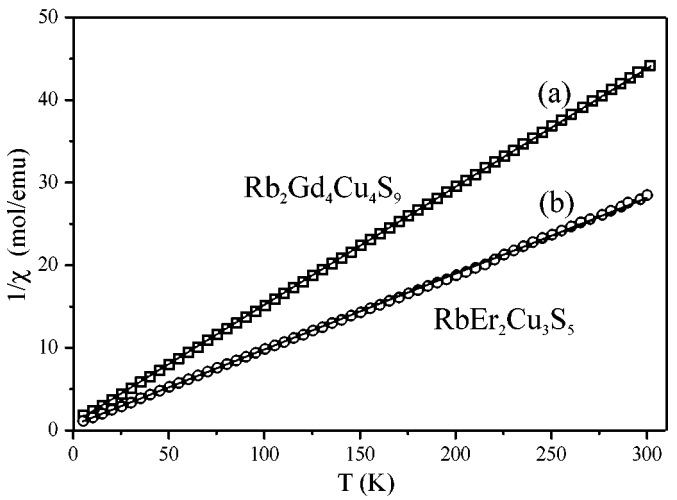

FIG. 11. Plots of the inverse molar susceptibility ($1/\chi$) vs *T* for (a) $Rb_2Gd_4Cu_4S_9$ and (b) $RbEr_2Cu_3S_5$, where the solid lines are the least-squares fit.

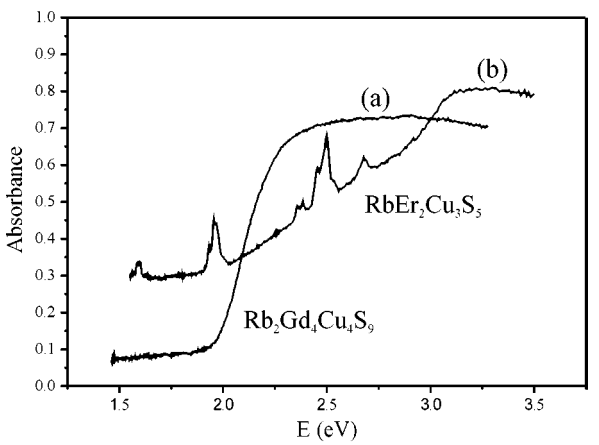

FIG. 12. Diffuse reflectance spectra of (a) $Rb_2Gd_4Cu_4S_9$ and (b) $RbEr_2Cu_3S_5$.

$^2_\infty[Ln_2Q_5]$ layers in ALn_2CuQ_4 and $Rb_2Gd_4Cu_4S_9$ are connected to their neighboring layers by the edge-sharing of two Q atoms to form the three-dimensional frameworks (Figs. 4 and 7), but such connections are not present in $ALn_2M_3Q_5$ (Fig. 6). In ALn_2CuQ_4 and $ALn_2M_3Q_5$ there is only one unique Ln atom and one unique $^1_\infty[Ln_2Q_6]$ chain, but in $Rb_2Gd_4Cu_4S_9$ there are two Gd atoms (Gd1, Gd2) and two chains. Each $^1_\infty[Ln_2Q_6]$ chain in ALn_2CuQ_4 is connected to two chains in the neighboring layers by edge-sharing (Fig. 4). Although the $^1_\infty[Gd1_2S_6]$ chain in $Rb_2Gd_4Cu_4S_9$ is not linked to other layers, each $^1_\infty[Gd2_2S_6]$ chain is connected to other layers (Fig. 7) in a manner similar to the $^1_\infty[Ln_2Q_6]$ chains in ALn_2CuQ_4. In going from $ALn_2M_3Q_5$ to $Rb_2Gd_4Cu_4S_9$ to ALn_2CuQ_4, the $Q:Ln$ ratio decreases. As a consequence, the linkages between the layers increase and the $^2_\infty[Ln_2Q_5]$ layer becomes more distorted, as shown in Figs. 4, 6, and 7. The $A:Ln$ ratio in the three structures is 1:2, but the $M:Ln$ ratio decreases from 3:2 to 1:1 to 1:2. In fact, the Ln/Q framework in $Rb_2Gd_4Cu_4S_9$ can be considered to be an intermediate phase.

In order to understand the coordination environments of M, Figs. 8, 9, and 10 show only M–Q bonds. ALn_2CuQ_4 contains some isolated Q^{2-} species and one-dimensional vertex-sharing MQ_4 tetrahedra that result in single $^1_\infty[CuQ_3]$ chains running along the [100] direction (Fig. 8) $ALn_2M_3Q_5$ contains single $^1_\infty[MQ_3]$ chains as well as double $^1_\infty[M_2Q_4]$ chains made up from two edge-sharing single $^1_\infty[MQ_3]$ chains; the single chains and double chains are connected together by vertex-sharing to form the two-dimensional $^2_\infty[M_3Q_5]$ layer (Fig. 9). $Rb_2Gd_4Cu_4S_9$ contains one-dimensional $^1_\infty[Cu_4S_8]$ chains made up of two single $^1_\infty[CuS_3]$ chains and one $^1_\infty[Cu_2S_4]$ double chain (Fig. 10).

Selected bond distances for $RbNd_2CuS_4$, $RbSm_2CuS_4$, $CsLa_2CuSe_4$, $CsSm_2CuSe_4$, $RbEr_2Cu_3S_5$, $CsGd_2Ag_3Se_5$, $CsTb_2Ag_3Se_5$, and $Rb_2Gd_4Cu_4S_9$ are listed in Tables 5, 6, and 7. In these structures all A atoms are in bicapped trigonal prisms of eight Q atoms with reasonable A–Q distances. Ln–Q distances are unexceptional and decrease from Nd to Er, as expected from the lanthanide contraction.

Plots of the reciprocal of the molar susceptibility ($1/\chi$) vs T for $Rb_2Gd_4Cu_4S_9$ and $RbEr_2Cu_3S_5$ are shown in Fig. 11. Both of these materials are paramagnetic in the range of $5-300$ K. The susceptibility data were fit by a least-squares method to the Curie–Weiss equation $\chi = C/(T-\theta)$, where C is the Curie constant and θ is the Weiss constant. The resulting values for C and θ are 7.8(1) emu K mol^{-1} and $-8.9(2)$ K for $Rb_2Gd_4Cu_4S_9$ and 11.12(4) emu K mol^{-1} and $-7.60(5)$ K for $RbEr_2Cu_3S_5$. The calculated effective magnetic moments of 7.9(2) μ_B and 9.43(5) μ_B agree well with the theoretical values of 7.94 μ_B and 9.58 μ_B for Gd^{3+} and Er^{3+}, respectively (24).

The diffuse reflectance spectra of $Rb_2Gd_4Cu_4S_9$ and $RbEr_2Cu_3S_5$ from 1.5 to 3.5 eV are shown in Fig. 12. An optical band gap of 1.94 eV for $Rb_2Gd_4Cu_4S_9$ was deduced with the use of a straightforward extrapolation method (25). This gap is consistent with the red color of the material. $RbEr_2Cu_3S_5$ exhibits a typical Er^{3+} absorption spectrum, with $4f-4f$ transitions at approximately 1.6, 1.9, and 2.5 eV.

ACKNOWLEDGMENTS

This research was supported by NSF Grant DMR97-09351. This work made use of Central Facilities supported by the MRSEC Program of the National Science Foundation (DMR00-76097) at the Materials Research Center of Northwestern University.

REFERENCES

1. S. A. Sunshine, D. Kang, and J. A. Ibers, *J. Am. Chem. Soc.* **109,** 6202–6204 (1987).
2. S. A. Sunshine, D. Kang, and J. A. Ibers, *Mater. Res. Soc. Symp. Proc.* **97,** 391–396 (1987).
3. F. Q. Huang and J. A. Ibers, *J. Solid State Chem.* **151,** 317–322 (2000).
4. J. A. Cody and J. A. Ibers, *Inorg. Chem.* **34,** 3165–3172 (1995).
5. A. E. Christuk, P. Wu, and J. A. Ibers, *J. Solid State Chem.* **110,** 330–336 (1994).
6. P. Wu, A. E. Christuk, and J. A. Ibers, *J. Solid State Chem.* **110,** 337–344 (1994).
7. P. Wu and J. A. Ibers, *J. Alloys Compd.* **229,** 206–215 (1995).
8. F. Q. Huang, W. Choe, S. Lee, and J. S. Chu, *Chem. Mater.* **10,** 1320–1326 (1998).
9. P. Wu and J. A. Ibers, *Z. Kristallogr.* **208,** 35–41 (1993).
10. P. Stoll, P. Dürichen, C. Näther, and W. Bensch, *Z. Anorg. Allg. Chem.* **624,** 1807–1810 (1998).
11. A. C. Sutorik, J. Albritton-Thomas, C. R. Kannewurf, and M. G. Kanatzidis, *J. Am. Chem. Soc.* **116,** 7706–7713 (1994).
12. W. Bensch and P. Dürichen, *Chem. Ber.* **129,** 1489–1492 (1996).
13. A. C. Sutorik, J. Albritton-Thomas, T. Hogan, C. R. Kannewurf, and M. G. Kanatzidis, *Chem. Mater.* **8,** 751–761 (1996).
14. R. Patschke, P. Brazis, C. R. Kannewurf, and M. Kanatzidis, *Inorg. Chem.* **37,** 6562–6563 (1998).
15. R. Patschke, J. Heising, and M. Kanatzidis, *Chem. Mater.* **10,** 695–697 (1998).
16. R. Patschke, P. Brazis, C. R. Kannewurf, and M. Kanatzidis, *J. Mater. Chem.* **8,** 2587–2589 (1998).
17. SMART, Version 5.054, Data Collection, and SAINT-Plus, Version 6.02A, Data Processing Software for the SMART System. Bruker Analytical X-Ray Instruments, Inc., Madison, WI, 2000.
18. G. M. Sheldrick, SHELXTL PC, Version 5.0, An Integrated System for Solving, Refining, and Displaying Crystal Structures from Diffraction Data. Siemens Analytical X-Ray Instruments, Inc., Madison, WI, 1994.
19. L. N. Mulay and E. A. Boudreaux (Eds.), "Theory and Applications of Molecular Diamagnetism." Wiley–Interscience, New York, 1976.
20. C. M. Plug and G. C. Verschoor, *Acta Crystallogr. B* **32,** 1856–1858 (1976).
21. P. M. Keane and J. A. Ibers, *Acta Crystallogr. C* **48,** 1301–1303 (1992).
22. S.-J. Kim, S.-J. Park, H. Yun, and J. Do, *Inorg. Chem.* **35,** 5283–5289 (1996).
23. M. Folchnandt and T. Schleid, *Z. Anorg. Allg. Chem.* **624,** 1595–1600 (1998).
24. W. E. Hatfield, *in* "Solid State Chemistry: Techniques" (A. K. Cheetham and P. Day, Eds.), pp. 122–162. Clarendon, New York, 1987.
25. O. Schevciw and W. B. White, *Mater. Res. Bull.* **18,** 1059–1068 (1983).